Topographic organization of single-neuron projectome for mouse prefrontal cortex

Jun Yan (junyan@ion.ac.cn)
Institute of Neuroscience, Chinese Academy of Sciences https://orcid.org/0000-0002-0405-0502

Le Gao
Institute of Neuroscience, Chinese Academy of Sciences

Sang Liu
Institute of Neuroscience, Chinese Academy of Sciences

Lingfeng Gou
Institute of Neuroscience, Chinese Academy of Sciences

Yachuang Hu
Institute of Neuroscience, Chinese Academy of Sciences

Yan-He Liu
Institute of neuroscience, CAS

Li Deng
Institute of Neuroscience, Chinese Academy of Sciences

Zhaoqin Chen
Chinese academy of sciences

Dechen Liu
Institute of Neuroscience, CAS Center for Excellence in Brain Science and Intelligence Technology, Chinese Academy of Sciences https://orcid.org/0000-0002-3907-1119

Shou Qiu
Institute of Neuroscience

Xiaofei Wang
Institute of Neuroscience, Chinese Academy of Sciences

Danying Wang
Institute of Neuroscience, Chinese Academy of Sciences

Xinran Wang
Institute of Neuroscience, Chinese Academy of Sciences

Biyu Ren
Institute of Neuroscience, Chinese Academy of Sciences

Qingxu Liu
Institute of Neuroscience, Chinese Academy of Sciences

Tianzhi Chen
Institute of Neuroscience, Chinese Academy of Sciences

Xiaoxue Shi
Institute of Neuroscience, Chinese Academy of Sciences
Haishan Yao
Institute of Neuroscience, CAS Center for Excellence in Brain Science and Intelligence Technology, Chinese Academy of Sciences https://orcid.org/0000-0003-4974-9197
Chun Xu
Institute of Neuroscience, State Key Laboratory of Neuroscience, Center for Excellence in Brain Science and Intelligence Technology, Chinese Academy of Sciences https://orcid.org/0000-0001-5149-8257
Cheng-Yu Li
Institute of Neuroscience, Chinese Academy of Sciences https://orcid.org/0000-0001-6829-0209
Anan Li
Wuhan National Lab for Optoelectronics, Huazhong University of Science & Technology
Qingming Luo
Hainan University https://orcid.org/0000-0002-6725-9311
Hui Gong
Huazhong University of Science and Technology https://orcid.org/0000-0001-5519-6248
Ning-long Xu
Institute of Neuroscience, CAS Center for Excellence in Brain Science and Intelligence Technology, Chinese Academy of Sciences https://orcid.org/0000-0002-1651-401X

Biological Sciences - Article

Keywords: High-level Cognitive Functions, Whole-brain Reconstruction, Axonal Morphologies, Projection Neurons, Arbor Distribution Analysis

Posted Date: December 18th, 2020

DOI: https://doi.org/10.21203/rs.3.rs-117637/v1

Abstract

Neurons in the prefrontal cortex (PFC) are responsible for high-level cognitive functions. Comparing to sensory and motor cortices, however, the connectivity organization of PFC is far more complex and still poorly understood. Here we report that whole-brain reconstruction of complete axonal morphologies of over 6,000 projection neurons in mouse PFC revealed fine-grained topographic relationship between the soma locations in PFC and their projection patterns before and after arriving the cortical and subcortical target regions. We first mapped the long-range projections of intratelencephalic (IT), pyramidal tract (PT), and corticothalamic (CT) neurons, and found that each class of these neurons can be further categorized into target-based subclasses, with somata of each subclass preferentially located at different PFC domains. Furthermore, the distribution of individual axon projections within each target region exhibited subregion preference, with their somata located in specific PFC subdomains. Mapping of single axons revealed a topographic order of primary axons within IT, PT, and CT fiber tracts that preserved the topography of their soma locations within PFC, and a spatial order of collateral branching points that yielded ordered clusters of collaterals aiming at specific targets. Within the target regions, we further observed subregion-specific arbor distribution that depended on the soma location. Such arbor distribution analysis of cortico-cortical PFC axons unveiled asymmetric terminal connectivity in PFC network. Our results demonstrate how large-scale single-neuron projectome analysis can provide new insights into the structural principle within the brain.

Introduction

Long-range projection neurons are essential for communication of neural information within the brain. Diverse patterns of axon projections are the basis of distinct neuronal functions, but the pattern of axon projection for single cortical neurons is only beginning to be elucidated by recent mesoscopic reconstruction studies[1,2]. In the neocortex, long-range projection neurons are broadly divided into three top-level neuron classes: intratelencephalic (IT) neurons, pyramidal tract (PT) neurons, and corticothalamic (CT) neurons, based on their projection patterns[3,4]. However, this classification is not sufficient to describe the functional and structural diversity of cortical projection neurons. For example, two subtypes of PT neurons in the motor cortex have been identified and shown to be involved in different aspects of motor functions[5]. To understand the full diversity of neuron types and the general rules of the connectivity organization requires extensive investigation of single neuron projectome within a brain region of interest. The prefrontal cortex (PFC) is believed to be responsible for high-level cognitive functions in mammalian brains and implicated in many neuropsychiatric diseases in humans[6]. It harbors diverse neuron subtypes that send axonal projections to numerous regions across the entire brain[7,8]. The complex connectivity patterns of PFC neurons, which are likely to reflect their diverse yet crucial functions, are still poorly understood due at least partially to the lack of systematic characterization at single-neuron level.

In this study, we reconstructed the axonal morphologies of over 6,000 individual projection neurons, covering extensively IT, PT, and CT neurons in PFC. Classification of axon projections revealed specific projection patterns that correlated systematically with the soma locations across PFC. Mapping the single-neuron projectome allowed us to reveal new PFC subdomains, modular connectivity within PFC, and subdivisions of PFC target regions. We unveiled a variety of rules underlying the projection diversity, including the ordered arrangement of primary axons, the selection of collaterals for target regions and the ordered distribution of axon arbors within target subregions. Analysis of the axon arbors identified the PFC loci with differential terminal innervation. This work illustrates the importance of large-scale single neuron projectome analysis for understanding the structural principle of long-range projections in the brain.

Results

Projectome Reconstruction of Single PFC Neurons

We sparsely labeled projection neurons of PFC[9] and imaged their whole-brain axon projections from a total of 149 mice using fluorescence Micro-Optical Sectioning Tomography (fMOST) technology[10,11] (**Fig. 1a, Supplementary Information 1,** Methods). We developed a software system, referred to as Fast Neurite Tracer (FNT), to streamline the tracing process of long-range axon projections in TB-sized light-microscopic datasets (**Extended Data Fig. 1**). Using FNT tracing pipeline, we reconstructed the axons of 6,101 projection neurons in mouse PFC. After registering all traced neuron projections to the Allen Brain Atlas (ABA) reference brain[12] (**Extended Data Fig. 2**), we found that the somata of traced PFC neurons were distributed across all PFC subregions (**Fig. 1b**) and they exhibited extensive and diverse projections in the whole brain (**Fig. 1c**). We then classified all traced neurons based on the result of global axon alignment by an algorithm referred to as FNT-dist (**Supplementary Information 2**) and visualized the results by t-distributed Stochastic Neighbor Embedding (t-SNE) (**Fig. 1d**). In line with the conventional definition of cortical projection neuron classes[3], these projection neurons can be readily divided into three main classes of IT, PT and CT neurons (**Fig. 1e**). Consistent with previous studies[13], the somata of IT, PT and CT neurons in PFC are preferentially distributed in different cortical layers, with IT mainly located in L2/3 and L5, PT in L5, and CT in L5/6 (**Fig. 1f**). Among all PFC neurons we analyzed, IT neurons are the most abundant, followed by PT and CT neurons. All our data can be visualized on the website: https://mouse.braindatacenter.cn/.

Target-based sub-classification of IT, PT, and CT neurons

We asked whether IT, PT and CT neurons in PFC can be further divided into subclasses, based on the pattern of their projection targets. For IT neurons, we first obtained six combinations of projections to cortex and striatum in each hemisphere (**Fig. 2a**). IT neurons with these different projection patterns can be found in all PFC regions but the proportions of these neurons vary across PFC regions and cortical layers (**Fig. 2b, c**). The somata of IT neurons projecting to contralateral cortex or striatum, or both are located in the deeper layers. Topographic relationships with additional IT neuron targets such as amygdala, pallidum, olfactory areas, claustrum, and endopiriform nucleus have also been found (**Extended Data Fig. 3a-c**). We further divided the projections of IT neurons into six patterns based on their ipsi- and contra-lateral cortical projections to PFC and non-PFC regions (**Fig. 2d**). Somata of neurons of these six patterns also showed different distributions across PFC regions and cortical layers (**Fig. 2e, f**). IT neurons with broader cortical projections such as those projecting outside of PFC are located in deeper layers than those projecting only locally within ipsilateral PFC. Meanwhile, IT neurons with contralateral projections showed high degree of symmetry between ipsi- and contra-lateral projections, with the extent of symmetry depended on the soma locations across PFC regions (**Extended Data Fig. 3d, e**). Finally, we focused on the IT neurons with long-range ipsilateral cortical projections outside PFC, and identified six subclasses of IT neurons (IT-1 to IT-6), each of which targeted a subset of 14 ipsilateral non-PFC cortical regions (**Fig. 2g**). Example neurons from different subclasses of neurons are illustrated in **Fig. 2h**. The somata of each subclass of IT neurons were largely preferentially distributed across PFC and cortical layers. For example, neurons of IT-1, IT-2, and IT-4 subclasses were differentially distributed in L5 and along dorsal to ventral direction in agranular insular cortex (**Fig. 2i**). The overall ipsilateral projections outside PFC from all PFC IT subclasses are summarized by the wiring diagram shown in **Fig. 2j**. Abbreviation of brain structures can be found in **Supplementary Information 3**.

Similarly, PFC PT and CT neurons mainly projecting to subcortical regions can be divided into 12 and six subclasses respectively based on their targets (**Extended Data Fig. 4a** and **Extended Data Fig. 5a**). The somata of each subclass of PT and CT neurons also showed distinct preference for PFC regions and cortical layers (**Extended Data Fig. 4b, c** and **Extended Data Fig. 5b, c**). For example, PT-4 neurons in ACAv (projecting to SCm) were distributed in superficial layer of L5 while PT-8 neurons in ACAv (projecting to Pons) were mainly in deep layer of L5 (**Extended Data Fig. 4d**), similarly for PT-2 and PT-11 in AId. As shown in **Extended Data Fig. 5b, c,** somata of the CT-1 subclass neurons (projecting to VAL, VM, and PCN) were mainly distributed in ACAd and deep layer of L5 while those of CT-2 subclass (projecting to LD and LP) mainly in ACAv and L6. Therefore, within each of IT, PT, and CT class, neurons can be further classified based on their projection patterns, and these new subclasses of neurons often exhibit differential preferences in their soma locations across PFC regions or cortical layers, or both. The functional relevance of these new PFC subclasses is shown in **Supplementary Information 4**.

Subdivision of PFC by single-neuron projectome

PFC is known to harbor subdomains with distinct functions[14] (**Supplementary Information 5**). Single-neuron projectome allowed us to subdivide PFC into subdomains systematically. To this aim, we investigated the spatial organization of PFC using the combined distributions of projection-defined subclasses for IT, PT and CT neurons across fine-grained PFC subregions. We unbiasedly divided PFC into a series of cortical columns (n=40) (Methods, **Fig. 3a**). We then obtained the spatial density distributions of all IT, PT, and CT subclasses among the cortical columns we defined. Using unsupervised hierarchical clustering, we found that PFC can be parcellated into medial (PFCm), lateral (PFCl), and dorsal (PFCd) subregions, each of which consists of a collection of cortical columns with similar compositions of PFC neuronal subclasses (**Fig. 3b, c**). Each projectome-defined PFC subregion encompasses several PFC regions defined in the ABA and a single PFC region in the ABA can span different projectome-defined PFC subregions (**Fig. 3d**). Furthermore, we constructed a network of intra-PFC connections among the cortical columns based on single-neuron projectome. We found that the intra-PFC connectivity network has a modular structure, in which the three modules are highly similar to the three subregions defined by PFC output projections (**Fig. 3e-g**). Further analysis of this modular structure unveiled connector hubs, non-hub connectors, provincial hubs and peripheral nodes[15]. Interestingly, we found that all cortical columns in PFCm are either connector hubs or non-hub connectors, underlining the role of PFCm as the main connector with PFCl and PFCd. Together, single-neuron projectome analysis reveals three PFC subregions defined by PFC output projections, a modular structure of intra-PFC connectivity, and the inter-modular connectors in PFC.

Subdivision of target regions by single-neuron projectome

Many PFC downstream target regions are known to have functional subdomains[7]. We next investigated whether different subdomains of a PFC target region can receive differential projections from different PFC neurons. Briefly, we divided the target region into a 3D collection of cubes and projection strength from each individual PFC neuron was quantified by the total axon length within the cube. The targeted subregions were determined by unsupervised hierarchical clustering of projection strengths among all cubes (**Fig. 3h**). As an example, the mediodorsal thalamus (MD) receives its majority of inputs from PFC. We first divided MD into five subdomains: anterior-medial (MDam), dorsal-anterior (MDda), dorsal-lateral (MDdl), central (MDc), and ventral-posterior (MDvp) subregions (**Fig. 3i, j**). This analysis also revealed the clustering of PFC neurons with distinct MD subregion preference (**Extended Data Fig. 6a, b**). We found that neurons in ORBm and ORBvl preferentially project to MDam, while neurons in AId project to MDvp. Thus, the distribution of PFC projections within MD exhibited a topographic order that reflect the topography of their somata in PFC. As MD receives projections from both CT neurons and PT neurons, we further found that topographic projections to MD are highly similar between the two neuron classes,

with CT projection generally stronger than PT projection (**Fig. 3k, l**). Using the same approach, we subdivided additional PFC downstream regions such as lateral hypothalamus (LHA) (**Extended Data Fig. 6c-g**). Taken together, with single-neuron projectome, we obtained detailed subdivision of PFC target regions in which we observed a clear topographic relationship with PFC soma location.

Primary axons and collaterals reflect soma topography and target locations

As single neurons utilize axon branching for target selection, we next characterized the patterns of axon branching of PFC neurons. Based on previous developmental studies of cortical neurons[16-19], we divided the axon projections into primary axons, axon collaterals, and terminal arbors (**Fig. 4a**, Methods). The primary axons of IT, PT and CT neurons form distinct fiber bundles (**Fig. 4b** and **Extended Data Fig. 7**). For PT neurons, the positions of primary axons on a series of cross-sections along the axon bundle remain positively correlated with soma locations, the extent of which decreases gradually as the axon bundle condenses and twists towards brain stem (**Fig. 4b, c**). We next clustered axon collaterals of PT neurons by FNT-dist into nine clusters, each of which extending towards a specific direction (**Fig. 4d**). The collateral branch points of these clusters are sequentially distributed on the primary axons with the order of branch points along primary axons positively correlated with the order of their respective target locations (**Fig. 4e-g**). Furthermore, the primary axons forming collaterals (e.g. those in collateral cluster 4) are generally closer to their respective target (SCm) than those primary axons that do not form collaterals (**Fig. 4h**). Finally, we found that the centers of axon arbors within the same target brain region (e.g. Striatum or Pons) are highly correlated with the branch point positions of collaterals within the same collateral cluster resulting in a more fine-grained soma-target topography (**Fig. 4i, j**). Therefore, axon collaterals of PT neurons form at ordered branch points along primary axons and are topographically organized to project to specific target locations.

Similarly, the primary axons of IT neurons within corpus callosum are topographically arranged and highly correlated with their homotypic targets in contralateral hemisphere (**Extended Data Fig. 7a, b**). We found IT collaterals sequentially targeting ipsilateral cortex, ipsilateral striatum, and contralateral targets along the primary axons (**Extended Data Fig. 7c**). Within ipsilateral cortex, IT collaterals were further sorted into clusters aiming at prefrontal, medial, somatomotor, and lateral cortical structures respectively, in line with our classification of IT neurons based on ipsilateral cortical projections (**Extended Data Fig. 7d-f** and **Fig. 2g**). The primary axons of CT neurons along medial to lateral direction turn roughly 90 degrees becoming anterior to posterior direction before arriving at thalamus and are highly correlated with their respective targets in thalamus (**Extended Data Fig. 7g-h**). Together, we found that the spatial arrangement of primary axons and collaterals of IT, PT and CT neurons reflects soma topography and target locations.

Spatial analysis of axon arbors reveals diverse modes of terminal innervation

The spatial distribution of axon terminals has important functional implications[4]. We obtained 56,825 terminal arbors using single-neuron reconstruction. We first explored the laminar distributions of 15,593 terminal arbors of IT neurons in the cortex. We classified these arbors into four subclasses (L1-, L2/3-, L5-, and L6-types) based on the arbor distribution across cortical layers (**Fig. 5a**). We found that the arbor type usage depends on the laminar location of soma with a positive correlation between soma depth and arbor depth across layers (**Fig. 5b**). We further found that the IT neurons in different PFC regions showed distinct arbor type preference, with the extend of preference further depended on the target identity (**Fig. 5c**). In general, projections from PFC to non-PFC regions use more L1- or L6-type arbors while intra-PFC projections use more L5-type arbors, in line with the current view of laminar patterns of feedback and feedforward projections[20]. Based on the patterns of arbor type usage, we classified all intra-PFC connections among cortical columns we defined in **Fig. 3a** into four classes, consistent between L2/3 and L5 neurons (**Fig. 5d** and **Extended Data Fig. 8a, b**). In particular, we identified significant differential usage of arbor types among all reciprocal connections among cortical columns **(Extended Data Fig. 8c)**. For example, the projections from column 28 (PFCd) to column 34 (PFCm) are enriched with L1-type arbors while the projections in opposite direction are enriched with L2/3- and L5-type arbors (**Fig. 5e-f**). Similar asymmetric arbor usage was found between column 7 (PFCl) and column 22 (PFCm). Notably, column 28, 34, 7 and 22 are all inter-modular connectors in intra-PFC connectivity network (**Fig. 3g**). Moreover, similar arbor types, soma-arbor relationship and patterns of arbor type usage have been found for 2,607 cortical terminal arbors of PT neurons, with PT neurons having more L5-type arbors than IT neurons (**Extended Data Fig. 8d-g**). Together, our arbor analysis suggested that previously reported laminar patterns of arbor terminations at population level[21] are in fact consisted of discrete arbor types at single-axon level and we mapped the precise loci with differential usage of arbor types, providing the directionality of inter-modular connectivity in PFC.

Furthermore, we analyzed arbor distributions of PT and CT neurons in thalamus (**Extended Data Fig. 9**). By clustering arbors based on their spatial overlaps, we identified subdomains within thalamus occupied by different arbor clusters (**Extended Data Fig. 9a, b**). Somata of neurons utilizing arbors in different arbor clusters are also preferentially distributed in different PFC regions (**Extended Data Fig. 9c, d**). We found that terminal arbors of PT and CT neurons in thalamus, known to function in “driver” and “modulator” modes respectively[22], are preferentially distributed in different arbor clusters (**Extended Data Fig. 9e**). Similar arbor organization has been found for PT and IT neurons in striatum (**Extended Data Fig. 10**). Therefore, axon arbors are spatially segregated within target brain regions in a manner depending on the

soma location, and the analysis of terminal arbors provides new insights into the functional diversity of terminal innervation.

Discussion

The information flows in the brain are facilitated by the axons that can extend to a long distance. However, how these long-range axons are spatially arranged in a highly compact brain to achieve the regulation of diverse targets is unknown. In this study, we reconstructed over 6,000 single-neuron projections in mouse PFC achieving a coverage comparable to current single-cell transcriptome studies. PFC has long been considered as the command center in the brain. Our study provided a comprehensive atlas of PFC projectome laying the structural foundation for studying diverse high-level cognitive functions. By analyzing single-neuron projectome, we unveiled a new brain map of PFC as well as PFC target regions beyond conventionally defined brain regions. Furthermore, our study suggests that topographic relationship with soma location is maintained at all levels of axon projections including primary axons, axon collaterals, and terminal arbors. These organizational principles are likely generalizable in the whole brain and could be fundamental to the parallel processing and integration of information in the mammalian brain.

Methods

Mice

Animal experimental procedures and care were approved by the Animal Care and Use Committee of the Center for Excellence in Brain Science and Intelligence Technology (Institute of Neuroscience), Chinese Academy of Sciences, Shanghai, China. All mice used in this study were C57BL/6 male mice (8 to 10 weeks old), purchased from SLAC laboratory, Shanghai. Mice were raised under the standard condition (12-hr light/dark cycle, 22-25°C) with the access to food and water *ad libitum*.

Virus injection

In order to achieve sparse labeling, a mixture of a diluted virus expressing Cre-recombinase (AAV2/8-hsyn-Cre-WPRE-pA, original titer: 1.4110^{13} V.G./ml) and a Cre-recombinase dependent reporter virus (AAV2/8-CAG-Flex-EGFP-WPRE-pA, original titer: 1.2510^{13} V.G./ml) were injected into the different PFC regions of adult C57BL/6 male mice. For each injection site, 20-50 nl of virus mixture was injected. The coordinates of stereotaxic injection were chosen according to The Mouse Brain in Stereotaxic Coordinates (second edition), measured in anterior-posterior (AP), medial-lateral (ML) and dorsal-ventral (DV) directions. The

angle of micro-injection is relative to vertical plane of DV axis. The Bregma point is defined as 0° (0, 0, 0) in the coordinate system of vertical injection. The detail information of injection can be found in **Supplement Information 1**.

fMOST imaging, data compression and image registration

All mouse brain samples in this study were imaged by fMOST technology as previously described[10,11]. The fMOST raw image data contain two channels: EGFP channel (for neurite tracing) and PI-staining channel (for image registration). A typical EGFP channel consists of around 10,000 16bit images in “tif” format of 30,00020,000 pixels in size. The raw data is processed into 1,000,000 data cubes of 256256100 voxels in size by FNT-slice2cube command. The data cubes were then compressed with HEVC method. We also downsampled the raw data to the resolution of 20μm20μm20μm for the overview of the whole brain data.

To map our reconstructed neurons onto Allen Brain Atlas (ABA) reference brain, we started with a rough registration from our PI-staining image (downsampled to 10μm10μm10μm) to ABA averaged template (10μm10μm10μm) by affine transformation including translation, rotation, scale and shear. We then manually segmented Isocortex, Hippocampal region, Caudoputamen, Thalamus and Hypothalamus in our data image. After that, we replaced the pixel values in the segmented areas of data image into the following values: 240, 80, 120, 160, 200 for Isocortex, Hippocampal region, Caudoputamen, Thalamus and Hypothalamus respectively. ABA template image was modified by the same operation. Next, we used nonrigid image registration method to map our modified data image to modified ABA template image[23] (**Extended Data Fig. 2d, e**). Finally, our reconstructed neurons were mapped onto ABA reference brain by calculated affine and nonrigid transformation accordingly (**Fig. 1c**). Affine registration and nonrigid registration were done by the software toolkit, Computational Morphometry Toolkit (CMTK).

Large-scale Single-neuron Reconstruction using Fast Neurite Tracer

Here we developed a new software tool, Fast Neurite Tracer (FNT), for efficiently tracing long-range axon projection, in tera-bytes of datasets generated by light microscopy. The workflow of FNT is shown in **Extended Data Fig. 1a**. The manual of FNT can be found in **Supplementary Information 7**. Briefly, to allow data loading into the memory of personal computer, original image data are split to smaller 3D data cubes by a program called “slice2cube” in FNT. For smooth transition during tracing, about eight

neighboring cubes around the current position are loaded into computer memory automatically. Loaded cubes are visualized in 3D for tracing. Users can conveniently switch to 2D visualization to examine the fine neuronal structures. Combined with zooming and rotation, it enhances human perception of complex 3D structures. **Extended Data Fig. 1b** shows the graphical user interface of FNT during tracing. To provide global perspective of original data, downsampled image data can be visualized simultaneously with the 3D data cube. To accommodate the experimental data with multi-color imaging such as PI staining in fMOST technology, FNT allows up to three sets of selected imaging data channels to be visualized at the same time. Categorical data such as brain annotation from Allen Brain Atlas (ABA) can also be incorporated. After loading the brain annotation file, the brain area annotation at any chosen position in the brain can be indicated.

FNT tracing process consists of three steps: finding a putative path, examining the putative path and extending the current neurite tree as summarized in **Extended Data Fig. 1c**. In FNT, we included a new operation: finding a putative path only with a starting position. In FNT, users' confirmation at each step ensures the correctness of tracing. After users confirm that a branch is traced to the end, the branch is marked as finished. FNT keeps the records of all unfinished branches and will automatically jump to the nearest unfinished branch when the current branch is finished. A neuron tree can be traversed in this way until it is completed (**Extended Data Fig. 1d**). Users can easily edit existing branches or undo previous unwanted operations. A demonstration of FNT tracing process is shown in **Supplementary Information 6**.

FNT allows distributed tracing of the same dataset by a large number of tracers simultaneously. Image data were compressed and can be accessed locally via portable hard disk or remotely through web-based computer network. We minimized the hardware requirement to allow users to run FNT on personal laptop computers. This allows us to conduct large-scale tracing through online crowdsourcing. We parallelly distributed the tracing tasks among a team of more than 70 human tracers. 7,000 neurons were traced using roughly 60,000 human hours over one year. Among 7,000 traced neurons, over 6,000 of them fall into PFC regions.

Quality controls and evaluation

To ensure the validity of tracing result, every neuron was traced by two independent human tracers. Then the results were merged by a third human tracer. We designed a scoring scheme combining different types of errors to evaluate the quality of tracing result. The penalties for 100-score are: false negative or false positive of branches (-2, n=1; -6, n=2 or 3; -11, n4), loop forming (-6), and mis-connections to other neurons (-11) (**Extended Data Fig. 2a**). We found that the merge of two independent tracing result can

significantly increase the quality score (**Extended Data Fig. 2b**). Among our traced neurons, we sampled 600 neurons for further evaluations by an independent team of tracers and found a median score of 94 for the tracing results of sampled neurons (**Extended Data Fig. 2c**).

Global alignment of single-neuron axons

We developed a dynamic programming algorithm, referred to as FNT-dist, to align axon projections of different neurons according to their morphology and geometry. The dissimilarities between the neurons were calculated by the alignment result. The detailed description of FNT-dist can be found in **Supplementary Information 2**.

Construction of PFC flatmap

For a better visualization of soma distribution in PFC, a flattened map of PFC was constructed. We first calculated the geodesic distance between each vertex on the surface of PFC and an anchor vertex. To project these vertices onto a 2D (U, V) coordinate system, we chose the anchor vertex as the origin, the medial-lateral axis as the U axis, and the anterior-posterior axis as the V axis. For every other vertex, we computed the directional vector to the anchor vertex on the horizontal plane and obtained the (U, V) coordinate by finding the location whose distance to the origin equals their geodesic distance along the directional vector.

Target-based sub-classification of IT, PT, and CT neurons

To construct the projection matrix for sub-classification of IT, PT, and CT neurons, we quantified the axonal length of every neuron in each target region. As the volume of each target region varies, we rescaled the projection matrix along target regions based on their minimal and maximal values. After obtaining the normalized projection matrix, we conducted unsupervised hierarchical clustering, using 1-Spearman correlation as the distance measure and Ward's linkage to identify target-based subclasses.

Construction of PFC columns

To unbiasedly divide PFC into a series of columns (n=40), voxels on the surface of PFC were clustered using K-means algorithm based on Euclidean distance between voxels. Then labels of voxels were propagated to entire PFC volume along the laminar direction based on the "streamline" method[12].

Subdivision of PFC

Sub-classification of IT, PT, and CT neurons revealed specific soma distribution for each subclass. For each constructed PFC column, we calculated the proportions of neuron subclasses in every neuron class (IT neurons, **Fig. 2g**; PT neurons, **Extended Data Fig. 4a**; CT neurons, **Extended Data Fig. 5a**). Then we conducted hierarchical clustering, using Spearman correlation as distance measure and Ward's linkage based on the distribution of proportions of neuronal subclasses in PFC columns (n=31). Columns 3, 4, 5, 8, 17, 21, 27, 29 and 31 containing less than 10 neurons were excluded from downstream analysis.

Subdivision of PFC target regions

For a given PFC target region such as MD, we first divided it into a series of 3D cubes (n=5,525 for MD, size: 505050 μm^3). Then for each neuron projecting to MD, we calculated the axonal length within each cube. After obtaining the projection matrix, we conducted unsupervised hierarchical clustering, using 1-Spearman correlation as distance measure and Ward's linkage to subdivide MD domains. To generate the map in **Fig. 3k** showing the soma distribution of neurons projecting to each MD subdomain, each MD-projecting neuron was color-coded by the specific MD subdomain receiving its strongest projection.

Identification of community and connector nodes in the intra-PFC network

We constructed the intra-PFC connectivity matrix based on the mean projection strength of neurons in each constructed PFC column. To investigate the modular structure of connectivity, we used the Louvain algorithm from Brain Connectivity Toolbox (https://sites.google.com/site/bctnet/)[24,25]. At each level of resolution with γ from 0 to 2 at the step size of 0.1, we ran the community detection algorithm for 1,000 times for the connectivity matrix and the shuffled matrix to determine the most consistent modular structures. The final modular structure was obtained at γ=1, where the difference of modularity value

between Q and $Q_{shuffled}$ is largest. The connectivity matrix was visualized in Gephi[26] and edges with projection strength less than 500 um was omitted (**Fig. 3e**). To identify the connector nodes, we computed the within-module strengths, and participation coefficients[15] for each node and the nodes with high participation coefficients were assigned as connectors.

Analysis of primary axons

In early brain development, the primary axons of IT, PT, and CT neurons extend towards contralateral hemisphere, spinal cord, and thalamus, respectively[16,18,19]. We thus designated the axon path from the soma to the most ventral branch point or axon end point within or near the midbrain as the primary axon of PT neurons. For IT neurons with contralateral projections, the axon path from the soma to the most lateral branch point or axon end point after crossing midline in either corpus callosum or anterior commissure was designated as the primary axon. For CT neurons, the path from the soma to the first branch point or axon end point entering the thalamus was designated as the primary axon.

After the designation of primary axons, we constructed a series of cross-sections with a step size of about 100 μm along primary axons. The direction of normal vector of each cross-section was chosen to be consistent with general direction of primary axon. The correlation between positions of somata and primary axons was calculated by the Pearson correlation between pairwise distances of somata and those of intersection points on each cross-section. The radius of the primary axon bundle was obtained by calculating the averaged distance from each intersection point to their center. Each cross-section was rotated around the axis perpendicular to their normal vector and the anterior-posterior axis to align the local coordinates of different cross-sections. We then used multiple linear regression to detect the most significant direction in which intersection points of primary axons are correlated with their soma location. The angle between the fitted direction in each cross-section was considered as the rotation angle along the primary axon bundle.

The clustering of collaterals

We obtained the collaterals by calculating the branch order for each neuron. The primary axon was assigned order as “1” and the branch orders of other branches were calculated based on branch angles. Branches were defined as symmetry branching if both daughter branches diverged with greater than 45° or the ratio of their branch angles is less than 1.7. In this case, the orders of both daughter branches were

designated as the branch order of their parent branch +1. Otherwise, branches were defined as collateral branching, in which the daughter branch with the smaller branching angle retained the same branch order as the parent branch while the other daughter branch was assigned as the branch order of their parent branch +1. The long branches with order of “2” were considered as collateral branches and classified into different collateral clusters by hierarchy clustering with Ward.2 method based on the dissimilarity scores obtained by the FNT-dist algorithm. The number of collateral clusters was determined by using the cutreeHybrid function[27] in the R package WGCNA, taking into account the branching structure of the hierarchical clustering tree while maximizing the between-cluster variation and minimizing within-cluster variation.

Detection of terminal arbors

As axon tree of a neuron is composed of connected nodes without loops, it can be viewed as a connected acyclic graph (i.e. a tree) and its terminal arbors can be viewed as its subgraphs. For an IT or PT neuron with complex structure, its branch points and end points excluding those on the primary axon were divided into several clusters by hierarchical clustering with the ward’s method based on their Euclidean distance. The number of clusters was determined by using the cutreeHybrid function in the R package WGCNA. A subgraph with nodes belonging to the same cluster was defined as a terminal arbor. Considering the simple structure of CT neurons, the subgraphs of a CT neuron after excluding its primary axon were directly defined as its terminal arbors.

Classification of cortical arbors

The projection strength in each cortical layer was defined as the total length of a terminal arbor within that layer and normalized by the maximum value. The similarity of laminar projection pattern between terminal arbors was calculated using Ward’s method with 1-Pearson correlations as the distance measure. The number of arbor clusters was determined by cutreeHybrid function in R. The classification of cortical connections followed the same pipeline. Intra-PFC cortico-cortical connections with no more than 10 terminal arbors were not considered in the analysis.

Quantification of spatial overlap between terminal arbor pairs

The coverage factor is a measure to quantify the overlap of two arbors, defined as the overlapped volume of two arbors divided by the mean of their volumes. The overlapped volume and the volume of each arbor were obtained by the intersectn function in the R package geometry. Terminal arbors in each brain region were divided into clusters by hierarchical clustering with Ward's method based on 1-Spearman rank correlation as the distance measure. The number of clusters was determined by cutreeHybrid function.

Data and code availability

All data can be found in the website: https://mouse.braindatacenter.cn/. The FNT software and the codes used in the data analysis can be found in the website: http://yanlab.org.cn.

Extended Figure Captions

Extended Data Figure 1. Design and application of FNT. (**a**) FNT workflow. (**b**) Graphic user interface during tracing. (**c**) Diagram of FNT tracing procedure. Red color denotes the operations that require precise mouse clicks. Orange color denotes the operations that require rotation, zooming in and out and users' observation. Green color denotes the operations that require a single key stroke. Green operations are much faster than the other operations. (**d**) An example showing consecutive steps (1-16) of tracing a neuron. Dashed arrows denote the automatic jumping from a finished branch to the nearest unfinished branch. (**e**) Pipeline of neurite tracing by multiple tracers.

Extended Data Figure 2. Quality controls, evaluation, speed of tracing and image registration. (**a**) Scoring scheme to evaluate the quality of neurite tracing. (**b**) Significant improvement of quality score after merging results from two independent annotators (n=13, two-sided Wilcoxon signed-rank test). (**c**) Distribution of quality scores of merged results for 600 randomly sampled neurons. (**d**) Accumulative numbers of traced neurons over time. (**e**) Pipeline of image registration. Step 1 involves affine registration and step 2 involves non-rigid registration. (**f**) Validation of image registration. Distance of mass center between brain structures (n=4) from different fMOST samples (n=5) were examined.

Extended Data Figure 3. Target-based sub-classification of IT neurons. (**a**) Laminar distribution of IT neurons projecting additional targets such as amygdala, pallidum, olfactory areas, claustrum, and endopiriform nucleus, with example neurons shown in (**b**). (**c**) Soma distribution of these neurons on PFC flatmap. (**d**) Ipsi- and contra-lateral projections of IT neurons in different PFC subregions. (**e**) Symmetry of ipsi- and contra-lateral projections of IT neurons. For each neuron, Pearson's correlation coefficient between ipsilateral projection (n=25) and contralateral projection (n=25) was computed as the symmetry index. Two-sided Wilcoxon signed-rank test was used to quantify the statistical significance of projection symmetry of neurons in each PFC subregion (*P<0.05, **P<0.01, ***P<0.001, ****P<0.0001).

Extended Data Figure 4. Target-based sub-classification of PT neurons. (**a**) 12 subclasses of PT neurons based on their projections to nine subcortical target regions, with their example neurons shown in (**b**) and soma distribution across PFC regions in (**c**). (**d**) The somata of PT-4 and PT-8 neurons defined in (**a**) showed different laminar distributions within ACAv. Similarly, the somata of PT-2 and PT-11 neurons showed different laminar distributions within AId.

Extended Data Figure 5. Target-based sub-classification of CT neurons. (**a**) Six subclasses of CT neurons based on their projections to 30 subcortical target regions, with their example neurons and soma distribution across PFC regions shown in (**b**). (**c**) The somata of CT-1 and CT-2 neurons defined in (**a**) showed regional differences along dorsoventral direction and different laminar distributions in ACAd and ACAv.

Extended Data Figure 6. Subdivision of PFC target regions by single-neuron projectome. (**a**) Heatmap of overall projection strengths from different PFC regions to MD subdomains. (**b**) Soma distribution of PFC neurons projecting to different MD subdomains. (**c**) Hierarchical clustering revealed four LHA domains: ventroposterior (LHAvp), anteriolateral (LHAal), central (LHAc), and dorsoposterior (LHAdp) subregions as shown in 3D view (**d**) and coronal sections (**e**). (f) Heatmap of projection strengths from different PFC regions to LHA subdomains. (**g**) Soma distribution of PFC neurons projecting to different LHA subdomains. Note that the neurons located in ACAd and ACAv preferentially project to LHAdp and neurons located in ORBvl preferentially project to LHAvp.

Extended Data Figure 7. Topographic organization of primary axons and axon collaterals for IT and CT neurons. (**a**) Primary axons of IT neurons and their target centers in the contralateral homotypic target region, color-coded according to the lateral to medial direction of their somata. (**b**) For IT neurons, the locations of somata, primary axons and collateral branch points are all highly correlated with their target centers within contralateral homotypic target region (all $P<2.210^{-16}$). (**c**) IT neuron collaterals targeting ipsilateral cortex, ipsilateral striatum, and contralateral targets branched out sequentially along the primary axons. (**d**) Axon collaterals of IT neurons are clustered into four clusters, each of which aims at different cortical target regions shown in (**e**). The enriched target regions for each collateral cluster were highlighted by black boxes ($P<0.0001$, one-sided Fisher's exact test). (**f**) Soma distributions of neurons containing collaterals in different collateral clusters. The brain regions enriched with neurons containing collaterals in each collateral cluster were highlighted by black boxes ($P<0.0001$, one-sided Fisher's exact test). (**g**) Primary axons and branch points of CT neurons and their target centers in thalamus, color-coded according to lateral to medial direction of their somata in PFC. The bold dark line indicates the

mean direction of primary axons, turning roughly 90 degrees when entering thalamus. (**h**) For CT neurons, the locations of somata and branch points are highly correlated with their target centers within thalamus (all $P<2.210^{-16}$).

Extended Data Figure 8. Analysis of arbor type usage of intra-PFC connections among cortical columns. (**a**) The patterns of arbor type usage of connections were clustered into four types. The averaged arbor type usage for each type of pattern was shown in **Fig. 5d**. The patterns of arbor type usage of connections for neurons located in L2/3, L5 respectively were also shown. Missing values (no such arbor type found) were colored in black. Note that the patterns of arbor type usage were similar between L2/3 and L5 neurons. (**b**) The mean relative depth of arbors in cortical layers from L2/3 neurons is positively correlated with the mean relative depth of arbors from L5 neurons across all connections ($P=6.110^{-9}$). (**c**) Heatmap of the statistical significance of differential arbor usage in all reciprocal connections calculated by $-\log_{10}(P)$ (Fisher's exact test, P value adjusted by Holm's method). Missing values (no reciprocal connections) were colored in black. (**d**) Clustering of cortico-cortical arbors of PFC PT neurons across cortical layers leads to four distinct arbor types, each of which specifically distributes in L1, L2/3, L5, and L6, similar to IT neurons. (**e**) Proportions of different arbor types used by IT and PT neurons located in different cortical layers. The enriched arbor type for IT and PT neurons were highlighted by black dots ($P<0.0001$, one-sided Fisher's exact test). (**f**) The patterns of arbor type usage of cortico-cortical projections are similar between L5 IT and PT neurons among projections of cortical columns. (**g**) The mean relative depth of arbors of IT neurons is positively correlated with the mean relative depth of arbors of PT neurons across all projections of cortical columns in (f) ($P=5.6\times10^{-6}$).

Extended Data Figure 9. Spatial analysis of terminal arbors of PFC neurons in thalamus. (**a**) The definition of coverage factor to quantify the spatial overlaps between two arbors. (**b**) Clustering of terminal arbors in thalamus leads to five arbor clusters based on the coverage factors between arbor pairs. (**c**) Each arbor cluster was segregated within thalamus and occupied different thalamic subregions as shown in (**d**). The enriched thalamic regions for each arbor cluster were highlighted by black dots ($P<0.0001$, one-sided Fisher's exact test). (**e**) Arbors of PT neurons and CT neurons were preferentially distributed in different arbor clusters. The neuron class (PT vs. CT) enriched in each arbor cluster was highlighted by black dots ($P<0.0001$, one-sided Fisher's exact test). (**f**) Soma distribution of neurons containing arbors in each arbor clusters across PFC regions. The PFC regions enriched with neurons containing arbors in each arbor cluster were highlighted by black dots ($P<0.0001$, one-sided Fisher's exact test).

Extended Data Figure 10. Spatial analysis of terminal arbors of PFC neurons in striatum. (**a**) Clustering of terminal arbors in striatum leads to six arbor clusters based on the coverage factors between arbor pairs. (**b**) Each arbor cluster was segregated within striatum and occupied different striatal subregions as shown in (**c**). The enriched striatal regions for each arbor cluster were highlighted by black dots (P<0.0001, one-sided Fisher's exact test). (**d**) Arbors of IT neurons and PT neurons were preferentially distributed in different arbor clusters. The neuron class (IT vs. PT) enriched in each arbor cluster was highlighted by black dots (P<0.0001, one-sided Fisher's exact test). (**e**) Soma distribution of neurons containing arbors in each arbor clusters across PFC regions. The PFC regions enriched with neurons containing arbors in each arbor cluster were highlighted by black dots (P<0.0001, one-sided Fisher's exact test).

Declarations

Acknowledgement

We thank Profs. Mu-ming Poo and Yangang Sun (Institute of Neuroscience, Chinese Academy of Sciences) for reading the manuscript and helpful discussions, Dr. Qiaoqiao Yang for editing the figures, Jing Xian (Shanghai JiGuang Polytechnic College), Yanqing Qiao, and numerous volunteers for testing FNT, and Jiawen Huang, Chenxi Jin, and Jiafei Wei for establishing the website for data browsing.

Author contributions

Design of the study, Jun Yan, Ninglong Xu, and Hui Gong; development of FNT, Lingfeng Gou; virus injection, Yanhe Liu, Li Deng, Qingxu Liu, Zhaoqin Chen, Tianzhi Chen, Dechen Liu, and Shou Qiu; project management, Danying Wang; data processing, quality control and management, Xiaofei Wang, Xinran Wang, Biyu Ren, and Xiaoxue Shi; fMOST imaging, Qingming Luo and Hui Gong; image preprocessing and quality control, Anan Li; image registration, Yachuang Hu; data analysis, interpretation and generation of figures, Le Gao, Sang Liu; writing, reviewing and editing the manuscript, Jun Yan, Ninglong Xu, Hui Gong, Le Gao and Sang Liu; scientific direction and funding, Jun Yan, Ninglong Xu, Hui Gong, Qingming Luo, Haishan Yao, Chun Xu, Chengyu T Li.

Funding

This work was supported by Shanghai Municipal Science and Technology Major Project Grant (No. 2018SHZDZX05), Strategic Priority Research Program of Chinese Academy of Sciences Grant (No. XDB32040100), and the National Natural Science Foundation of China Grant (Nos. 61890953, 81827901).

Declaration of Interests

The authors declare no competing interests.

References

1 Han, Y. *et al.* The logic of single-cell projections from visual cortex. *Nature* **556**, 51-56, doi:10.1038/nature26159 (2018).

2 Winnubst, J. *et al.* Reconstruction of 1,000 Projection Neurons Reveals New Cell Types and Organization of Long-Range Connectivity in the Mouse Brain. *Cell* **179**, 268-281 e213, doi:10.1016/j.cell.2019.07.042 (2019).

3 Gerfen, C. R., Economo, M. N. & Chandrashekar, J. Long distance projections of cortical pyramidal neurons. *J Neurosci Res* **96**, 1467-1475, doi:10.1002/jnr.23978 (2018).

4 Harris, K. D. & Shepherd, G. M. The neocortical circuit: themes and variations. *Nat Neurosci* **18**, 170-181, doi:10.1038/nn.3917 (2015).

5 Economo, M. N. *et al.* Distinct descending motor cortex pathways and their roles in movement. *Nature* **563**, 79-84, doi:10.1038/s41586-018-0642-9 (2018).

6 Carlen, M. What constitutes the prefrontal cortex? *Science* **358**, 478-482, doi:10.1126/science.aan8868 (2017).

7 Gabbott, P. L., Warner, T. A., Jays, P. R., Salway, P. & Busby, S. J. Prefrontal cortex in the rat: projections to subcortical autonomic, motor, and limbic centers. *J Comp Neurol* **492**, 145-177, doi:10.1002/cne.20738 (2005).

8 Zhang, S. *et al.* Organization of long-range inputs and outputs of frontal cortex for top-down control. *Nat Neurosci* **19**, 1733-1742, doi:10.1038/nn.4417 (2016).

9 Xu, N. L. *et al.* Nonlinear dendritic integration of sensory and motor input during an active sensing task. *Nature* **492**, 247-251, doi:10.1038/nature11601 (2012).

10 Gong, H. *et al.* High-throughput dual-colour precision imaging for brain-wide connectome with cytoarchitectonic landmarks at the cellular level. *Nat Commun* **7**, 12142, doi:10.1038/ncomms12142 (2016).

11 Wang, X. *et al.* Chemical sectioning fluorescence tomography: high-throughput, high-contrast, multicolor, whole-brain imaging at subcellular resolution. *Cell Reports*, doi:10.2139/ssrn.3677215 (2020) (accepted).

12 Wang, Q. *et al.* The Allen Mouse Brain Common Coordinate Framework: A 3D Reference Atlas. *Cell* **181**, 936-953 e920, doi:10.1016/j.cell.2020.04.007 (2020).

13 Shepherd, G. M. Corticostriatal connectivity and its role in disease. *Nat Rev Neurosci* **14**, 278-291, doi:10.1038/nrn3469 (2013).

14 Zingg, B. *et al.* Neural networks of the mouse neocortex. *Cell* **156**, 1096-1111, doi:10.1016/j.cell.2014.02.023 (2014).

15 Guimera, R. & Nunes Amaral, L. A. Functional cartography of complex metabolic networks. *Nature* **433**, 895-900, doi:10.1038/nature03288 (2005).

16 O'Leary, D. D. *et al.* Target selection by cortical axons: alternative mechanisms to establish axonal connections in the developing brain. *Cold Spring Harb Symp Quant Biol* **55**, 453-468, doi:10.1101/sqb.1990.055.01.045 (1990).

17 Luo, L. & O'Leary, D. D. Axon retraction and degeneration in development and disease. *Annu Rev Neurosci* **28**, 127-156, doi:10.1146/annurev.neuro.28.061604.135632 (2005).

18 Deck, M. *et al.* Pathfinding of corticothalamic axons relies on a rendezvous with thalamic projections. *Neuron* **77**, 472-484, doi:10.1016/j.neuron.2012.11.031 (2013).

19 Kalil, K. & Dent, E. W. Branch management: mechanisms of axon branching in the developing vertebrate CNS. *Nat Rev Neurosci* **15**, 7-18, doi:10.1038/nrn3650 (2014).

20 Felleman, D. J. & Van Essen, D. C. Distributed hierarchical processing in the primate cerebral cortex. *Cereb Cortex* **1**, 1-47, doi:10.1093/cercor/1.1.1 (1991).

21 Harris, J. A. *et al.* Hierarchical organization of cortical and thalamic connectivity. *Nature* **575**, 195-202, doi:10.1038/s41586-019-1716-z (2019).

22 Sherman, S. M. Thalamus plays a central role in ongoing cortical functioning. *Nat Neurosci* **19**, 533-541, doi:10.1038/nn.4269 (2016).

23 Rohlfing, T. & Maurer, C. R., Jr. Nonrigid image registration in shared-memory multiprocessor environments with application to brains, breasts, and bees. *IEEE Trans Inf Technol Biomed* **7**, 16-25,

doi:10.1109/titb.2003.808506 (2003).

24 Rubinov, M. & Sporns, O. Complex network measures of brain connectivity: uses and interpretations. *Neuroimage* **52**, 1059-1069, doi:10.1016/j.neuroimage.2009.10.003 (2010).

25 Blondel, V. D., Guillaume, J. L., Lambiotte, R. & Lefebvre, E. Fast unfolding of communities in large networks. *J Stat Mech-Theory E*, doi:Artn P10008

10.1088/1742-5468/2008/10/P10008 (2008).

26 Bastian, M., Heymann, S. & Jacomy, M. in *International AAAI Conference on Weblogs and Social Media* (2009).

27 Langfelder, P., Zhang, B. & Horvath, S. Defining clusters from a hierarchical cluster tree: the Dynamic Tree Cut package for R. *Bioinformatics* **24**, 719-720, doi:10.1093/bioinformatics/btm563 (2008).

Figures

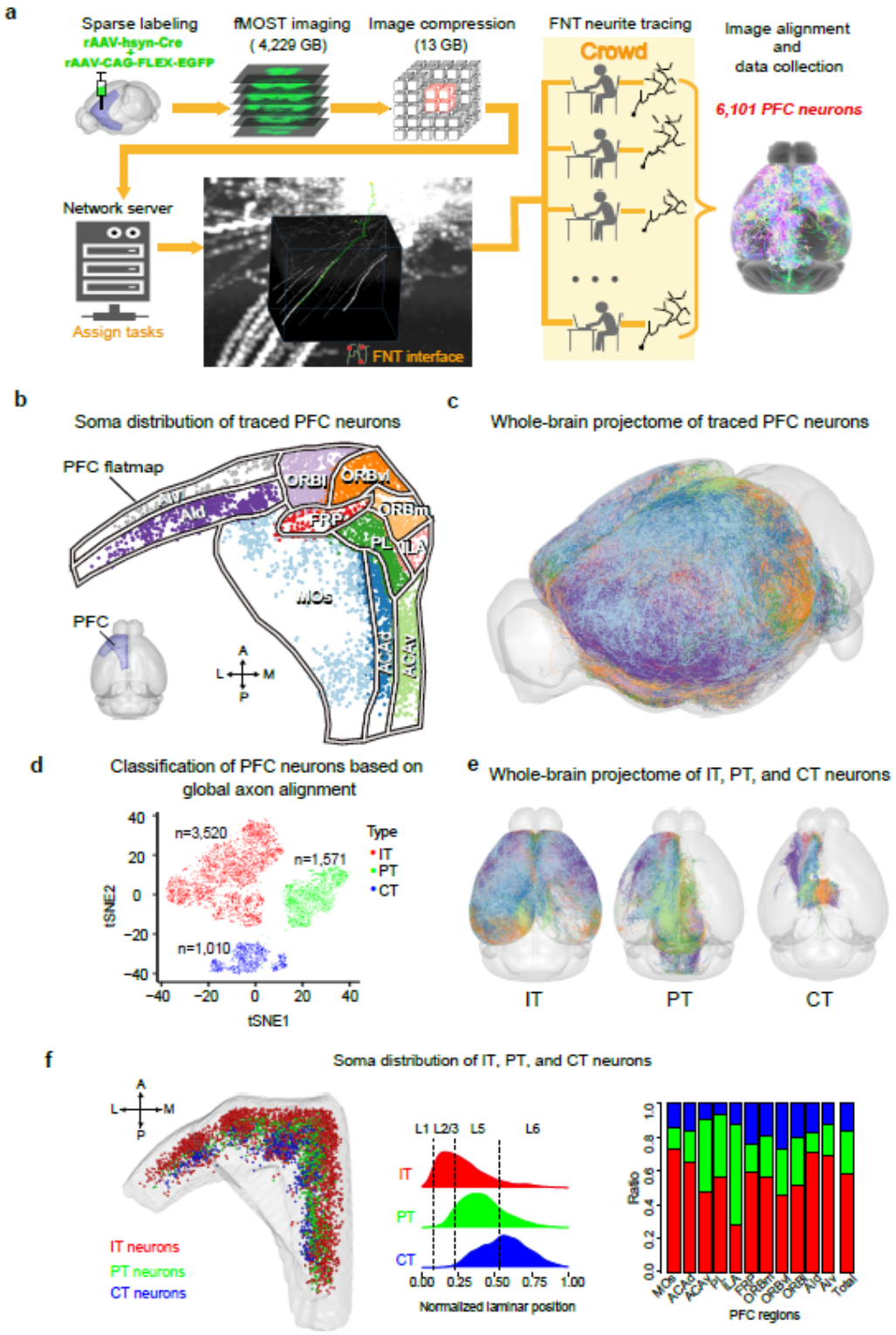

Figure 1

Reconstruction of PFC single-neuron projectome. (a) The pipeline of PFC single-neuron projectome reconstruction including sparse labeling, fMOST imaging, image compression, tracing using FNT, image alignment and data collection. (b) Soma distribution of traced PFC neurons shown on a PFC flatmap. Somata of neurons were color-coded for different PFC regions. (c) Whole-brain projectome of all traced PFC neurons, with their axons color-coded according to their somata in (b). (d) T-SNE plot of all classified

IT, PT, and CT neurons according to the global alignment of axons. (e) Whole-brain projectome of IT, PT, and CT neurons. (f) Soma distribution of IT, PT, and CT neurons across laminar layers and different PFC regions. Three classes of neurons showed progressively deeper laminar distributions and similar relative abundances across different PFC regions.

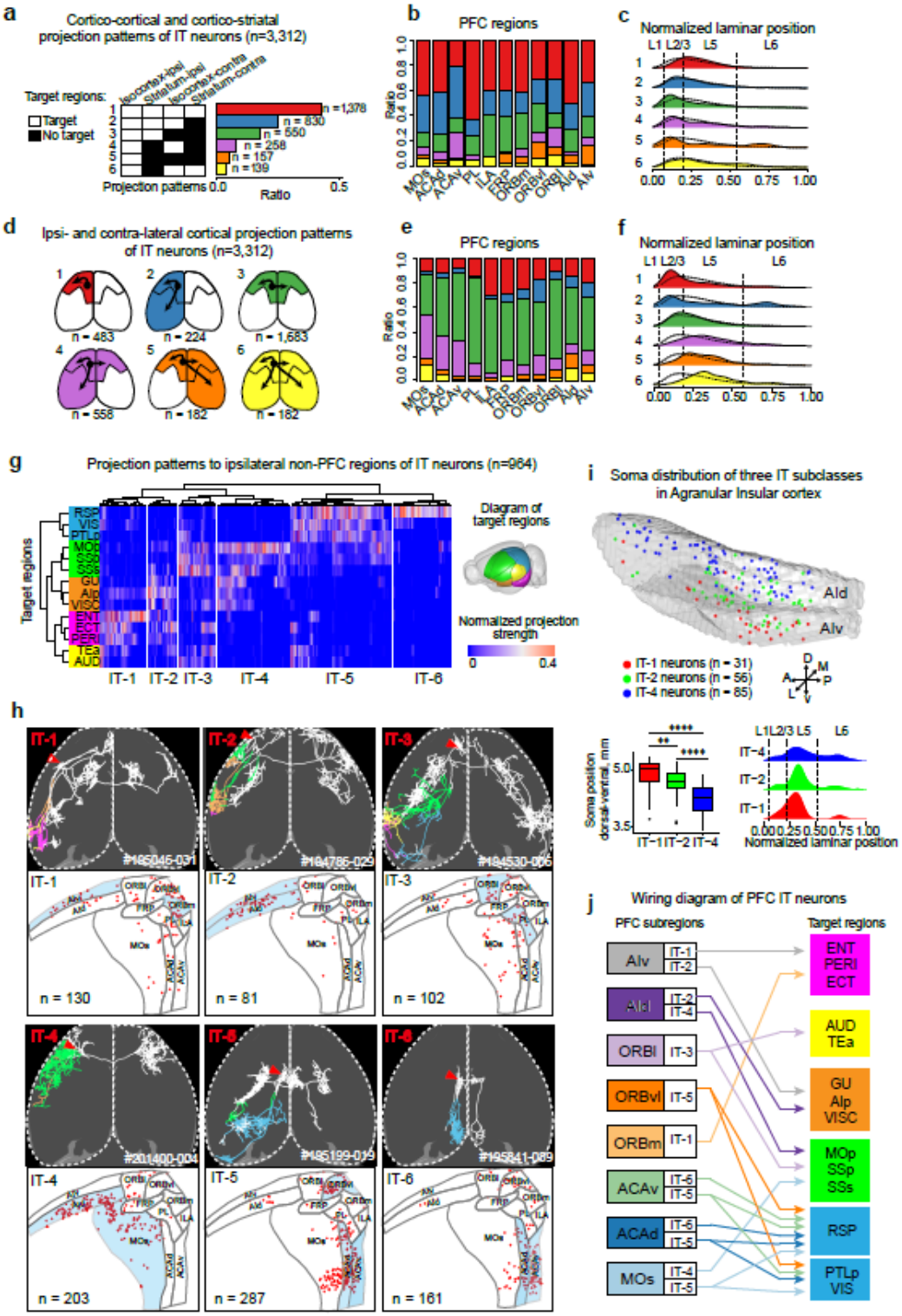

Figure 2

Target-based sub-classification of IT neurons. (a) Six combinatorial patterns of corticocortical and corticostriatal projections of IT neurons, with their soma distributions across PFC regions (b) and laminar layers (c). The grey dashed line denotes the laminar distribution of all neurons serving as a background. (d) Six patterns of ipsi- and contra-lateral cortical projections of IT neurons based on their targets in PFC vs. non-PFC regions, with their soma distribution across PFC regions (e) and laminar layers (f). (g) Six subclasses of IT neurons based on their ipsilateral projections to 14 non-PFC regions, with their example neurons and soma distribution across PFC regions shown in (h). Target regions were grouped and colored according to the hierarchical clustering. The red arrow in (h) denotes the location of soma and axon segments were colored according to target regions. The light-blue shaded regions shown in PFC flatmap denote the areas of clustered neurons. (i) The somata of IT-1, IT-2, and IT-4 neurons defined in (g) show regional differences along dorsoventral direction and different laminar distributions within AId and AIv (two-sided Wilcoxon signed-rank test, *P<0.05, **P<0.01, ***P<0.001, ****P<0.0001). (j) Subclass-specific wiring diagram of IT neurons in the cortex.

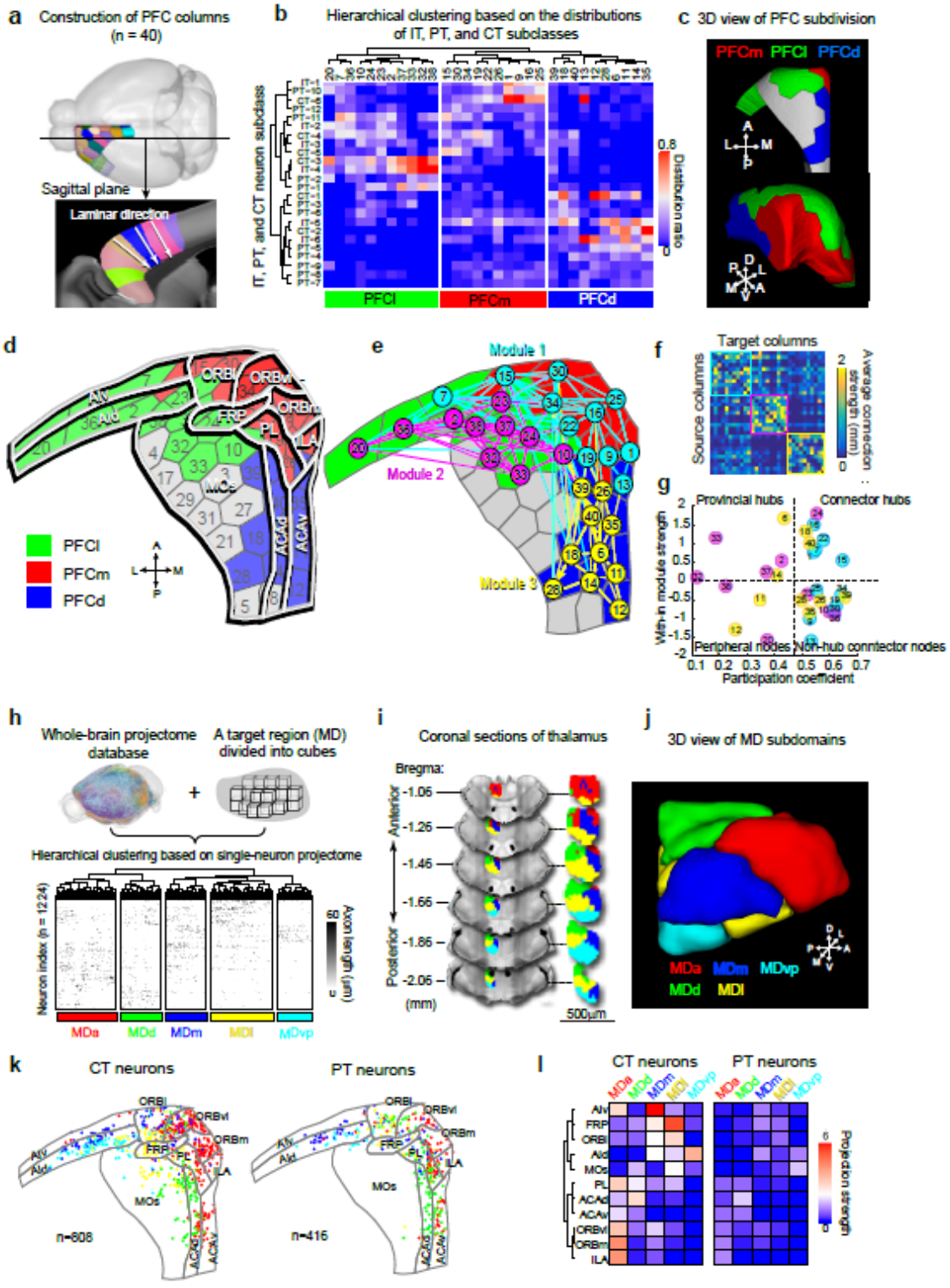

Figure 3

Subdivision of PFC and PFC target regions by single-neuron projectome. (a) Our schema to subdivide PFC into 3D columns (Methods). Columns were randomly colored and a sagittal plane was shown to illustrate that the shape of columns along the laminar direction. (b) Heatmap showing the clustering result of 3D columns using overall compositions of IT, PT, and CT subclasses (IT-1 to IT-6, PT-1 to PT-12, CT-1 to CT-6). Three subdomains were revealed: lateral PFC (PFCl), medial PFC (PFCm), and dorsal PFC

(PFCd). (c) 3D view of subdivided PFC subdomains in (b). (d) Comparison between projectome-based PFC subdivision with ABA PFC regions shown in a flatmap. (e) Three modules of strong intra-PFC connections identified by the clustering of intra-PFC connectivity matrix (f). (g) Classification of network nodes in (e) based on within module strength and participation coefficients (Methods). (h) Our schema to subdivide a given target region by single-neuron projectome using MD as an example. (i) Subdivided MD subdomains shown on a series of coronal sections and in 3D (j). (k) Soma distributions of CT and PT neurons projecting to different MD subdivisions shown on PFC flatmap. (l) Comparison of projection strengths of CT and PT neurons to MD subdomains from different PFC regions.

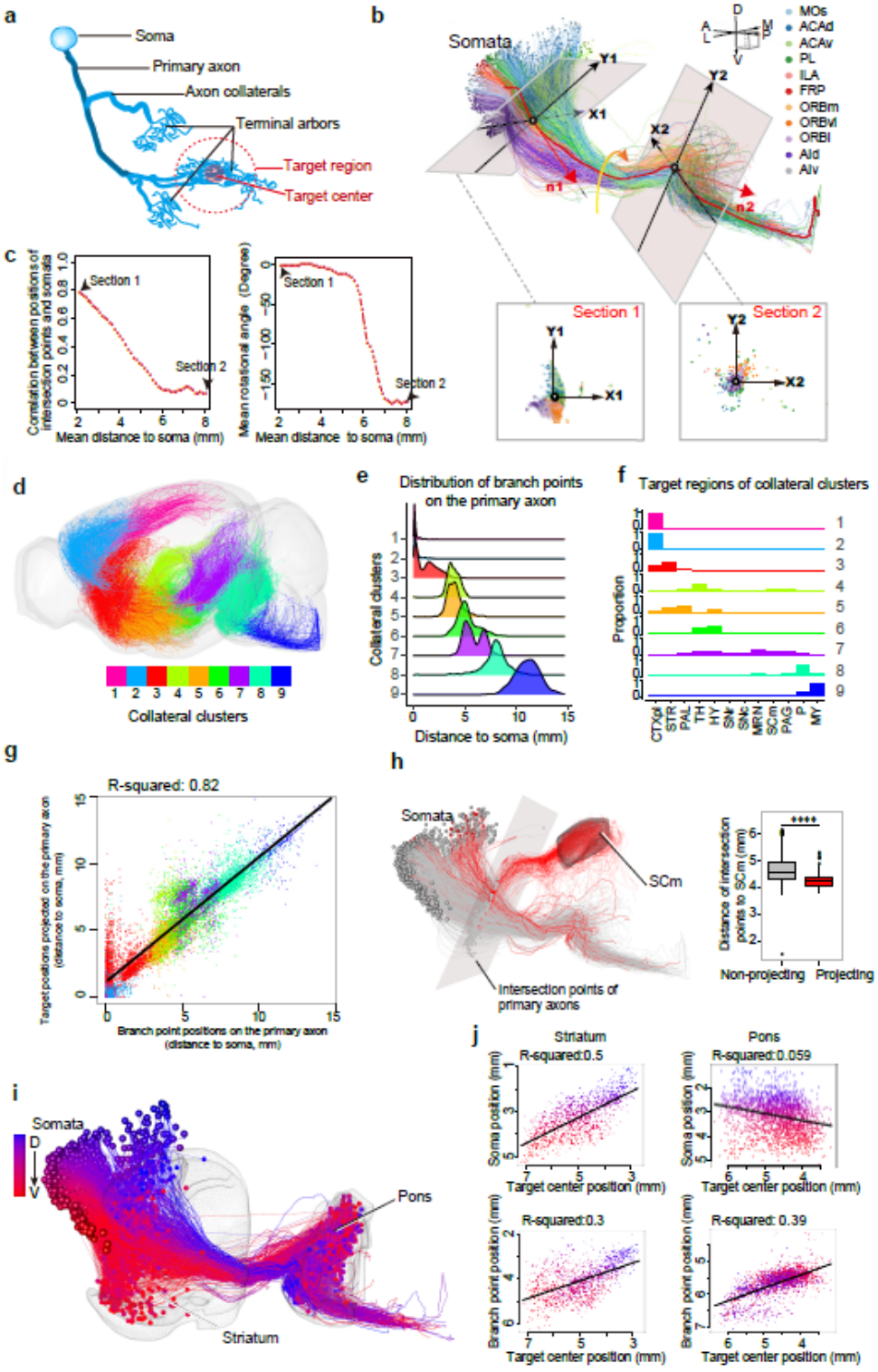

Figure 4

Topographic organization of primary axons and axon collaterals for PT neurons. (a) Our schema to divide single-neuron projectome into primary axons, axon collaterals, and terminal arbors. (b) Primary axons are color-coded according to the brain regions where their somata are located. The red dotted line denotes the mean centers of primary axons. Two cross-sections are shown with their local coordinates (X1, Y1 and X2, Y2) and their normal vectors (n1 and n2). The yellow arrow indicates the direction of

rotation. Inset: intersection points of primary axons in each cross-section. (c) Correlation between the positions of intersection points and soma locations, and mean rotational angles calculated at a series of cross-sections along PT fiber tract. (d) Axon collaterals are clustered into nine clusters. (e) Collaterals in each cluster branch out at distinct locations along primary axons and aim at different brain regions shown in (f). (g) Branch point positions and target positions projected on the primary axons (i.e. the nearest points on the primary axon to their perspective targets) are positively correlated ($P<2.2\times10^{-16}$). (h) Within collateral cluster 4 shown in (d), primary axons that form collaterals to SCm (red) are closer to SCm than those do not (grey) on the cross-section plane near the collateral branch points (two-sided Wilcoxon signed-rank test, ****$P<0.0001$). (i) Distribution of somata of PT neurons and their target centers in striatum and pons along dorsoventral direction. (j) The locations of somata and collateral branch points in collateral cluster 3 and 8 are highly correlated with their target centers within striatum and pons respectively. The correlations were calculated along the dorsal-ventral direction of somata, collateral branch points, and their target centers (all $P<2.2\times10^{-16}$).

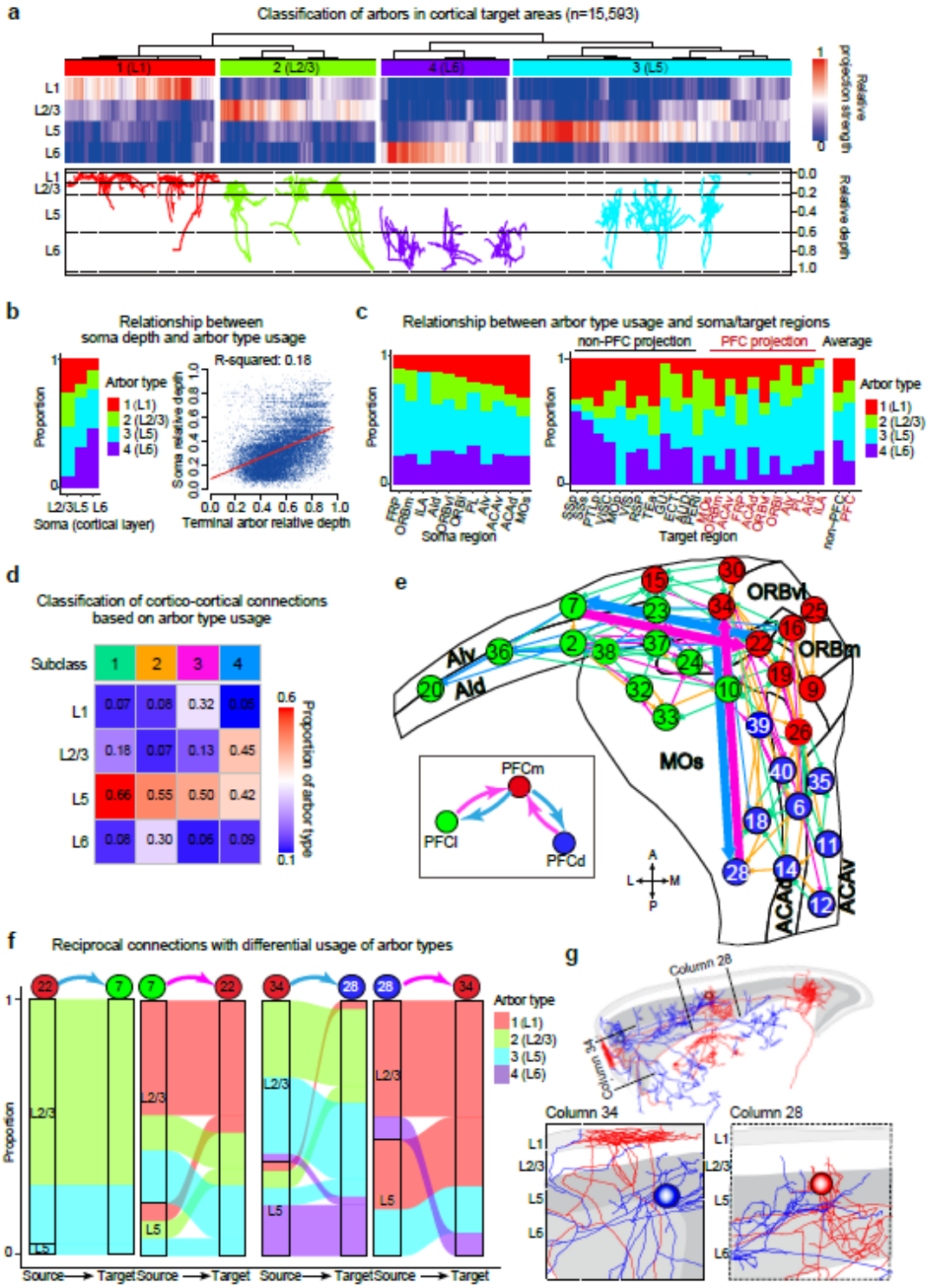

Figure 5

Spatial analysis of terminal arbors of PFC cortico-cortical projections. (a) Clustering of terminal arbors of PFC IT neurons across cortical layers leads to four distinct arbor types each of which specifically distributes in L1, L2/3, L5, and L6, with example arbors shown below. (b) Proportions of different arbor types used by neurons located in different cortical layers and the correlation between soma depth and terminal arbor depth across cortical layers (P<2.2×10-16). (c) Proportions of different arbor types used by

neurons located in different PFC regions and in different cortical target regions, with PFC regions colored in red. (d) Four patterns of intra-PFC connections among cortical columns based on arbor type usage. (e) Intra-PFC cortical connectivity network. Each connection was colored by the pattern of arbor type usage in (d). The width of connection represents the statistical significance of asymmetry in reciprocal connections given by -log10(P) (Fisher's exact test, P value adjusted by Holm's method). The widths of non-reciprocal connections were set to the minimum value of 0.01. $P<1\times10\text{-}5$ for the connections between column 7 and 22, and for column 28 and 34. Inset: a simplified model of asymmetric intra-PFC connectivity. (f) Proportions of arbor types for neurons located in different layers of cortical column 7 and 22, and column 28 and 34 involved in their reciprocal connections. (g) Two example neurons in column 28 and 34 with asymmetric arbor usage in their reciprocal connections. Inset: enlarged view of column 28 and 34.

Supplementary Files

This is a list of supplementary files associated with this preprint. Click to download.

- 1mouseandinjectioninformation.xlsx
- 2supplementarymethodsofFNTv2.pdf
- 3abbreviationsofbrainstructures.pdf
- 4functionalrelevanceofITPTandCTneuronsubclasses.pdf
- 5diversefunctionsofPFCsubregionscuratedfromtheliterature.pdf
- 6FNTtracingprocedures.mp4
- 7usermanualofFNT.pdf
- ExtendedDataFigure1.pdf
- ExtendedDataFigure2.pdf
- ExtendedDataFigure3.pdf
- ExtendedDataFigure4.pdf
- ExtendedDataFigure5.pdf
- ExtendedDataFigure6.pdf
- ExtendedDataFigure7.pdf
- ExtendedDataFigure81128.pdf
- ExtendedDataFigure9.pdf
- ExtendedDataFigure10.pdf